Thermo-mechanical analysis of laminated composite and sandwich beams based on a variables separation.

P. Vidal, L. Gallimard, O. Polit

Thermo-mechanical analysis of laminated composite and sandwich beams based on a variables separation

P. Vidal *, L. Gallimard, O. Polit

Laboratoire Energétique, Mécanique, Electromagnétisme, Université Paris Ouest Nanterre-La Défense, 50 rue de Sèvres, 92410 Ville d'Avray, France

A B S T R A C T

In this paper, a finite element based on the variables separation is presented for the thermo-mechanical analysis of bi-dimensional laminated beams. Both the temperature and displacement fields are approximated as a sum of separated functions of x (axial coordinate) and z (transverse coordinate). This choice yields to an iterative process that consists of computing a product of two one-dimensional functions at each iteration. A fourth-order expansion with respect to the thickness direction are considered. The capability and the behavior of the presented approach are shown on various laminated and sandwich beams submitted to different thermal boundary conditions. Thermal and mechanical responses are assessed by comparing with other approaches available in literature, exact solutions and 2D finite element computation.

1. Introduction

Composite and sandwich structures are widely used in industrial field due to their excellent mechanical properties. In this context, they can be submitted to severe conditions which imply to take into account thermal effects. In fact, they can play an important role on the behavior of structures in services, which leads to evaluate precisely their influence on stresses, particularly at the layer interfaces.

The aim of this paper is to construct an accurate and efficient approach for analyzing laminated beams including thermomechanical effects in elasticity for small displacements. As pointed out in [1], it is important to consider the real distribution of the temperature issued from the heat conduction problem.

From the literature, various mechanical models for composite or sandwich beams were extended to include thermal effects. It is well-established that they can be classified as Equivalent Single Layer (ESL) or Layerwise (LW) models. In the first one, the number of unknowns are independent of the number of layers, but the shear stress continuity at the layer interfaces are often violated. We can find the classical laminate theory [2], the first order shear deformation theory ([3] with a linear variation of temperature through the thickness), and higher order theories [4,5] for thermal stresses analysis of beams or plates. The LW approach aims at overcoming the restriction of the ESL. Lee has included the thermal effect for beam structures in [6]. Unfortunately, the cost increases with the number of plies. Carrera [7,8] has presented various ESL and LW theories with mixed and displacement-based approaches for assumed distribution of temperatures (uniform, linear, localized) in the framework of the Carrera's Unified Formulation (CUF). A family of higher-order beam elements has been derived with different displacement field approximations over the cross-section. The Fourier heat conduction problem is solved analytically and a Navier-type closed form solution with radial basis function is obtained in [9]. As an alternative, refined models have been developed in order to improve the accuracy of ESL models avoiding the additional computational cost of LW approach. Based on physical considerations and after some algebraic transformations, the number of unknowns becomes independent of the number of layers. In this framework, Kapuria used a zigzag theory for displacements for beams in [10]. A piecewise linear function along the thickness is used for the temperature. A global–local approach in conjunction with a Hermite interpolation of the temperature through the thickness is carried out in [11]. For an overview about the thermal analysis, see for example [4,12–14].

Over the past years, the Proper Generalized Decomposition (PGD) has shown interesting features in the reduction model framework [15]. It has been used in the context of coordinate variables separation in multi-dimensional PDEs [15]. In particular, it has been applied for composite beams in [16] and plates based on Navier-type solution in [17] or using finite element (FE) method in [18,19]. Concerning the thermal problem, it has been adressed in

* Corresponding author.
E-mail address: philippe.vidal@u-paris10.fr (P. Vidal).

[20]. For a review about the PGD and its fields of applications, the reader can refer to [21,22].

So, the aim of the present work is to extend the previously developed method to take into account the thermo-mechanical coupling for laminated composite and sandwich beams. In this way, the temperature and the displacements are written under the form of a sum of products of unidimensional polynomials of x and z. For the mechanical unknowns, a piecewise fourth-order Lagrange polynomial of z is chosen as it is particularly suitable for such laminated structures (see [19]). The temperature unknowns are also interpolated with the same order expansion. As far as the variation with respect to the axial coordinate is concerned, a 1D three-node FE is employed. Using this method, each unknown function of x is classically approximated using one degree of freedom (dof) per node of the mesh and the LW unknown functions of z are global for the whole beam. Finally, the deduced thermal and mechanical non-linear problems imply the resolution of two linear problems alternatively. This process yields to two 1D problems in which the number of unknowns is much smaller than a classical Layerwise approach. It should be noted that weakly coupled problems are studied. The thermal problem is first solved, and then the solution of the mechanical problem is obtained considering the temperature distribution as a load. As the temperature unknowns are expressed under a separated form, the variables separation of the mechanical part remains unchanged. Moreover, the approach allows us to refine easily the description of the temperature variation without increasing significantly the computational cost which is important to derive an accurate mechanical response.

We now outline the remainder of this article. First, the thermo-mechanical formulation is given. In particular, the heat conduction problem and the coupling behavior law are recalled. Then, the resolution of the thermal problem based on the variables separation is described and the FE discretization is given. Finally, it is illustrated by numerical tests involving thermal loads and thermo-mechanical coupling. They have been performed upon various laminated and sandwich beams for different boundary conditions. The behavior of the method is discussed. It is assessed by comparing with classical LW approach, exact solutions and also 2D FEM computations issued from a commercial finite element software. These examples show the efficiency and the accuracy of the presented approach.

2. Thermo-mechanical problem description

Let us consider a beam occupying the domain $\mathcal{B} = \mathcal{B}_x \times \mathcal{B}_z \times \left[-\frac{b}{2} \leqslant y \leqslant \frac{b}{2}\right] = [0, L] \times \left[-\frac{h}{2} \leqslant z \leqslant \frac{h}{2}\right] \times \left[-\frac{b}{2} \leqslant y \leqslant \frac{b}{2}\right]$ in a Cartesian coordinate (x, y, z). The beam has a rectangular uniform cross section of height h, width b and is assumed to be straight. The beam is made of NC layers of different linearly elastic materials. Each layer may be assumed to be orthotropic in the beam axes. The x axis is taken along the central line of the beam whereas y and z are the two axes of symmetry of the cross section intersecting at the centroid, see Fig. 1. As shown in this figure, the y axis is along the width of the beam. This work is based upon a displacement approach for geometrically linear elastic beams.

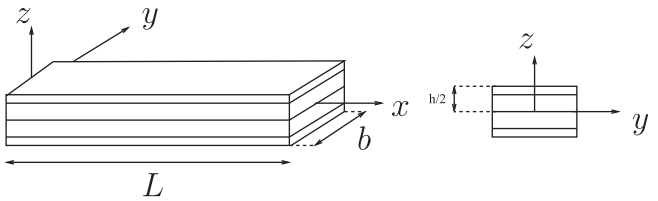

Fig. 1. The laminated beam and co-ordinate system.

In the following, the beam is considered in the (x, z) plane as a plane stress assumption is used.

2.1. Heat conduction problem

2.1.1. Thermal constitutive relation

The physical problem considered here involves the two-dimensional linear heat conduction equations with thermal conductivity components λ_1, λ_3 in the x, z directions respectively. The constitutive equation is given by the Fourier law:

$$\mathbf{Q} = \begin{bmatrix} q_1 \\ q_3 \end{bmatrix} = \bar{\boldsymbol{\lambda}}\, \mathbf{grad}(\theta) \tag{1}$$

where

$$\bar{\boldsymbol{\lambda}} = \begin{bmatrix} \lambda_1 & 0 \\ 0 & \lambda_3 \end{bmatrix} \text{ and } \mathbf{grad}(\theta) = \begin{bmatrix} \theta_{,x} \\ \theta_{,z} \end{bmatrix}$$

q_i $(i = 1, 3)$ is the heat flux components with respect to the coordinate system x, z respectively. $\theta_{,x}$, $\theta_{,z}$ stand for the derivative of θ with respect to x and z respectively.

2.1.2. The weak form of the boundary value problem

For $\delta\theta \in \delta\Theta$ $(\delta\Theta = \{\theta \in H^1(\mathcal{B})/\theta = 0 \text{ on } \partial\mathcal{B}_\theta\})$, the variational principle is given by: find $\theta \in \Theta$ such that:

$$-\int\int_{\mathcal{B}} \mathbf{grad}(\delta\theta)^T \mathbf{Q}(\theta)\, d\mathcal{B} + \int\int_{\mathcal{B}} \delta\theta r_d\, d\mathcal{B} + \int_{\partial\mathcal{B}_h} \delta\theta h_d\, d\partial\mathcal{B} = 0 \quad \forall \delta\theta \in \delta\Theta \tag{2}$$

where r_d and h_d are the prescribed volume heat source and surface heat flux applied on $\partial\mathcal{B}_h$ respectively. Θ is the space of admissible temperatures, i.e. $\Theta = \{\theta \in H^1(\mathcal{B})/\theta = \theta_d \text{ on } \partial\mathcal{B}_\theta\}$.

In the present work, the convection heat transfer is not considered.

2.2. Thermo-mechanical problem

2.2.1. Constitutive relation

The reduced two dimensional constitutive law of the kth layer with thermo-mechanical coupling is given by

$$\boldsymbol{\sigma}^{(k)} = \overline{\mathbf{C}}^{(k)} \left(\boldsymbol{\varepsilon}^{(k)} - \bar{\boldsymbol{\alpha}}^{(k)} \Delta\theta^{(k)} \right) \tag{3}$$

The stress and strain tensor can be written as

$$\boldsymbol{\sigma}^T = [\sigma_{11}\ \sigma_{33}\ \tau_{13}], \quad \boldsymbol{\varepsilon}^T = [\varepsilon_{11}\ \varepsilon_{33}\ \gamma_{13}]$$

We have also

$$\overline{\mathbf{C}}^{(k)} = \begin{bmatrix} \overline{C}_{11}^{(k)} & \overline{C}_{13}^{(k)} & 0 \\ & \overline{C}_{33}^{(k)} & 0 \\ symm & & \overline{C}_{55}^{(k)} \end{bmatrix}$$

where $\overline{C}_{ij}^{(k)}$ are the moduli of the material for the kth layer taking into account the zero transverse normal stress hypothesis $(\sigma_{22} = 0)$. They are expressed by

$$\overline{C}_{ij}^{(k)} = C_{ij}^{(k)} - C_{i2}^{(k)} C_{j2}^{(k)} / C_{22}^{(k)} \tag{4}$$

where $C_{ij}^{(k)}$ are orthotropic three-dimensional elastic moduli. We also have $\overline{C}_{55}^{(k)} = C_{55}^{(k)}$.

The vector $\bar{\boldsymbol{\alpha}}^{(k)^T} = [\alpha_1^{(k)}\ \alpha_3^{(k)}\ 0]$ contains the thermal expansion coefficients.

2.2.2. The weak form of the boundary value problem

Using the above notation and Eq. (3), the variational principle is given by:

Find $\mathbf{u}(M) \in U$ (space of admissible displacements) such that

$$\int\int_{\mathcal{B}} \delta\boldsymbol{\varepsilon}^T \overline{\mathbf{C}}^{(k)} \boldsymbol{\varepsilon}\ dV = \int\int_{\partial\mathcal{V}_F} \delta\mathbf{u}\cdot\mathbf{t}\ dS + \int\int_{\mathcal{B}} \delta\boldsymbol{\varepsilon}^T \overline{\mathbf{C}}^{(k)} \bar{\boldsymbol{\alpha}}^{(k)} \Delta\theta\ dV \quad \forall \delta u \in \delta U \tag{5}$$

where $\mathbf{t}$ is the prescribed surface forces applied on $\partial\mathcal{V}_F$. The body forces are not considered in this expression.

3. Application of the variables separation to the thermo-mechanical analysis of beam

The Proper Generalized Decomposition (PGD) was introduced in [15] and is based on an *a priori* construction of separated variables representation of the solution. For the thermal analysis, the solution with separated coordinate variables has been developed in [20]. In the present scope, a weak thermo-mechanical coupling is considered, the resolution process is divided into 2 steps. First, the thermal problem is solved by introducing the separated representation in Eq. (2). It will be described in the following sections. Then, the mechanical response is deduced from the resolution of Eq. (5) following [16]. It will not be detailed hereafter for brevity reason.

3.1. The temperature field

The temperature solution $\theta(x,z)$ is constructed as the sum of N products of functions of only one spatial coordinate ($N \in \mathbb{N}$ is the order of the representation) such that:

$$\theta(x,z) = \sum_{i=1}^{N} T_x^i(x) T_z^i(z) \tag{6}$$

where $T_z^i(z)$ is defined in $\mathcal{B}_z$ and $T_x^i(x)$ is defined in $\mathcal{B}_x$. A classical quadratic FE approximation is used in $\mathcal{B}_x$ and a LW description is chosen in $\mathcal{B}_z$ as it is particulary suitable for the modeling of composite structures.

The expression of the gradient of the temperature is given as follows:

$$\mathbf{grad}(\theta) = \sum_{i=1}^{N} \begin{bmatrix} T_{x,x}^i(x) T_z^i(z) \\ T_x^i(x) T_{z,z}^i(z) \end{bmatrix} \tag{7}$$

3.2. The problem to be solved

The resolution of Eq. (2) is based on a greedy algorithm. If we assume that the first m functions have been already computed, the trial function for the iteration $m+1$ is written as

$$\theta^{m+1}(x,z) = \theta^m(x,z) + T_x(x) T_z(z) \tag{8}$$

where T_x and T_z are the functions to be computed and θ^m is the associated known sets at iteration m defined by

$$\theta^m(x,z) = \sum_{i=1}^{m} T_x^i(x) T_z^i(z) \tag{9}$$

The test function is

$$\delta(T_x T_z) = \delta T_x . T_z + T_x . \delta T_z \tag{10}$$

The test function defined by Eq. (10), the trial function defined by Eq. (8) are introduced into the weak form Eq. (2) to obtain the two following equations, where the prescribed volume and surface heat source are assumed to be nill:

$$\int_{\mathcal{B}_x}\int_{\mathcal{B}_z} \mathbf{grad}(\delta T_x T_z)^T \bar{\boldsymbol{\lambda}} \mathbf{grad}(T_z T_x)\ dz\,dx = -\int_{\mathcal{B}_x}\int_{\mathcal{B}_z} \mathbf{grad}(\delta T_x T_z)^T \bar{\boldsymbol{\lambda}} \mathbf{grad}(\theta^m)\ dz\,dx \tag{11}$$

$$\int_{\mathcal{B}_z}\int_{\mathcal{B}_x} \mathbf{grad}(\delta T_z T_x)^T \bar{\boldsymbol{\lambda}} \mathbf{grad}(T_x T_z)\ dx\,dz = -\int_{\mathcal{B}_z}\int_{\mathcal{B}_x} \mathbf{grad}(\delta T_z T_x)^T \bar{\boldsymbol{\lambda}} \mathbf{grad}(\theta^m)\ dx\,dz \tag{12}$$

From Eqs. (11) and (12), a coupled non-linear problem is derived. Thus, a non linear resolution strategy has to be used. The simplest one is a fixed point method. An initial function $T_x^{(0)}, T_z^{(0)}$ is set, and at each step, the algorithm computes two new pairs $(T_x^{(k+1)}, T_z^{(k+1)})$ such that

- $T_x^{(k+1)}$ satisfies Eq. (11) for T_z sets to $T_z^{(k)}$
- $T_z^{(k+1)}$ satisfies Eq. (12) for T_x sets to $T_x^{(k+1)}$

These two equations are linear and the first one is solved on $\mathcal{B}_x$, while the second one is solved on $\mathcal{B}_z$. The fixed point algorithm is stopped when

$$\frac{\|T_x^{(k+1)} T_z^{(k+1)} - T_x^{(k)} T_z^{(k)}\|_{\mathcal{B}}}{\|T_x^{(0)} T_z^{(0)}\|_{\mathcal{B}}} \leqslant \varepsilon \tag{13}$$

where $\|A\|_{\mathcal{B}} = \left[\int_{\mathcal{B}_x}\int_{\mathcal{B}_z} A^2\,dx\,dz\right]^{1/2}$ and ε is a small parameter to be fixed by the user. In this paper we set $\varepsilon = 10^{-6}$.

Remark. When a prescribed temperature is imposed on $\partial\mathcal{B}_\theta$, the first couple is built so as to fulfill this requirement. Then, the following couples are computed satisfying a zero temperature on $\partial\mathcal{B}_\theta$.

3.3. Finite element discretization

To build the beam finite element approximation, a discrete representation of the functions (T_x, T_z) must be introduced. We use classical finite element approximation in $\mathcal{B}_x$ and $\mathcal{B}_z$. The elementary vectors of degree of freedom (dof) associated with the finite element mesh in $\mathcal{B}_x$ and $\mathcal{B}_z$ are denoted $\mathbf{q}_e^x$ and $\mathbf{q}_e^z$, respectively. The temperature fields and the associated gradient are determined from the values of $\mathbf{q}_e^x$ and $\mathbf{q}_e^z$ by

$$\begin{aligned} T_{xe} &= \mathbf{N}_x \mathbf{q}_e^x, \quad \boldsymbol{\mathcal{E}}_x^e = \mathbf{B}_x \mathbf{q}_e^x, \\ T_{ze} &= \mathbf{N}_z \mathbf{q}_e^z, \quad \boldsymbol{\mathcal{E}}_z^e = \mathbf{B}_z \mathbf{q}_e^z, \end{aligned} \tag{14}$$

where $\boldsymbol{\mathcal{E}}_x^{eT} = [T_{x,x} \quad T_x]$ and $\boldsymbol{\mathcal{E}}_z^{eT} = [T_z \quad T_{z,z}]$. The matrices $[\mathbf{N}_x], [\mathbf{B}_x], [\mathbf{N}_z], [\mathbf{B}_z]$ contain the interpolation functions, their derivatives and the jacobian components dependent on the chosen discrete representation.

3.4. Finite element problem to be solved on $\mathcal{B}_x$

For the sake of simplicity, the function $T_z^{(k)}$ which is assumed to be known, will be denoted $\widetilde{T}_z$, and the function $T_x^{(k+1)}$ to be computed will be denoted T_x. The gradient in Eq. (11) is defined as

$$\mathbf{grad}(\widetilde{T}_z T_x) = \boldsymbol{\Sigma}_{\mathbf{z}}(\widetilde{T}_z) \boldsymbol{\mathcal{E}}_x \tag{15}$$

with

$$\boldsymbol{\Sigma}_{\mathbf{z}}(\widetilde{T}_z) = \begin{bmatrix} \widetilde{T}_z & 0 \\ 0 & \widetilde{T}_{z,z} \end{bmatrix} \tag{16}$$

The variational problem defined on $\mathcal{B}_x$ from Eq. (11) is

$$\int_{\mathcal{B}_x} \delta\mathcal{E}_x^T \boldsymbol{\lambda}_z(\widetilde{T}_z) \mathcal{E}_x dx = -\int_{\mathcal{B}_x} \delta\mathcal{E}_x^T \mathbf{Q}_z(\widetilde{T}_z, \theta^m) dx \tag{17}$$

with

$$\boldsymbol{\lambda}_z(\widetilde{T}_z) = \int_{\mathcal{B}_z} \boldsymbol{\Sigma}_{\mathbf{z}}(\widetilde{T}_z)^T \bar{\boldsymbol{\lambda}} \boldsymbol{\Sigma}_{\mathbf{z}}(\widetilde{T}_z) dz \tag{18}$$

$$\mathbf{Q}_z(\widetilde{T}_z, \theta^m) = \int_{\mathcal{B}_z} \boldsymbol{\Sigma}_{\mathbf{z}}(\widetilde{T}_z)^T \bar{\boldsymbol{\lambda}} \mathbf{grad}(\theta^m) dz \tag{19}$$

The introduction of the finite element approximation Eq. (14) in the variational Eq. (17) leads to the linear system

$$\boldsymbol{\Lambda}_z(\widetilde{T}_z)\,\mathbf{q}^x = \boldsymbol{\mathcal{R}}_x(\widetilde{T}_z, \theta^m) \tag{20}$$

where $\mathbf{q}^x$ is the vector of the nodal temperatures associated with the finite element mesh in $\mathcal{B}_x$, $\boldsymbol{\Lambda}_z(\widetilde{T}_z)$ the conductivity matrix obtained by summing the elements' conductivity matrices $\boldsymbol{\Lambda}^e_z(\widetilde{T}_z)$ and $\boldsymbol{\mathcal{R}}_x(\widetilde{T}_z, \theta^m)$ the equilibrium residual obtained by summing the elements' residual load vectors $\boldsymbol{\mathcal{R}}^e_x(\widetilde{T}_z, \theta^m)$

$$\boldsymbol{\Lambda}^e_z(\widetilde{T}_z) = \int_{L_e} \mathbf{B}_x^T \boldsymbol{\lambda}_z(\widetilde{T}_z) \mathbf{B}_x dx \tag{21}$$

and

$$\boldsymbol{\mathcal{R}}^e_x(\widetilde{T}_z, \theta^m) = -\int_{L_e} \mathbf{B}_x^T \mathbf{Q}_z(\widetilde{T}_z, \theta^m) dx \tag{22}$$

3.5. Finite element problem to be solved on $\mathcal{B}_z$

For the sake of simplicity, the function $T_x^{(k+1)}$ which is assumed to be known, will be denoted $\widetilde{T}_x$, and the function $T_z^{(k+1)}$ to be computed will be denoted T_z. The gradient in Eq. (12) is defined as

$$\mathbf{grad}(\widetilde{T}_x T_z) = \boldsymbol{\Sigma}_{\mathbf{x}}(\widetilde{T}_x)\boldsymbol{\mathcal{E}}_z \tag{23}$$

with

$$\boldsymbol{\Sigma}_{\mathbf{x}}(\widetilde{T}_x) = \begin{bmatrix} \widetilde{T}_{x,x} & 0 \\ 0 & \widetilde{T}_x \end{bmatrix} \tag{24}$$

The variational problem defined on $\mathcal{B}_z$ from Eq. (12) is

$$\int_{\mathcal{B}_z} \delta\mathcal{E}_z^T \boldsymbol{\lambda}_x(\widetilde{T}_x)\mathcal{E}_z dz = -\int_{\mathcal{B}_z} \delta\mathcal{E}_z^T \mathbf{Q}_x(\widetilde{T}_x, \theta^m) dz \tag{25}$$

with

$$\boldsymbol{\lambda}_x(\widetilde{T}_x) = \int_{\mathcal{B}_x} \boldsymbol{\Sigma}_{\mathbf{x}}(\widetilde{T}_x)^T \bar{\boldsymbol{\lambda}} \boldsymbol{\Sigma}_{\mathbf{x}}(\widetilde{T}_x) dx \tag{26}$$

$$\mathbf{Q}_x(\widetilde{T}_x, \theta^m) = \int_{\mathcal{B}_x} \boldsymbol{\Sigma}_{\mathbf{x}}(\widetilde{T}_x)^T \bar{\boldsymbol{\lambda}} \mathbf{grad}(\theta^m) dx \tag{27}$$

The introduction of the finite element discretization Eq. (14) in the variational Eq. (25) leads to the linear system

$$\boldsymbol{\Lambda}_x(\widetilde{T}_x)\,\mathbf{q}^z = \boldsymbol{\mathcal{R}}_z(\widetilde{T}_x, \theta^m) \tag{28}$$

where $\mathbf{q}^z$ is the vector of the nodal temperature associated with the finite element mesh in $\mathcal{B}_z$, $\boldsymbol{\Lambda}_x(\widetilde{T}_x)$ the conductivity matrix obtained by summing the elements' conductivity matrices $\boldsymbol{\Lambda}^e_x(\widetilde{T}_x)$ and $\boldsymbol{\mathcal{R}}_z(\widetilde{T}_x, \theta^m)$ the equilibrium residual obtained by summing the elements' residual load vectors $\boldsymbol{\mathcal{R}}^e_z(\widetilde{T}_x, \theta^m)$

$$\boldsymbol{\Lambda}^e_x(\widetilde{T}_x) = \int_{Lz_e} \mathbf{B}_z^T \boldsymbol{\lambda}_x(\widetilde{T}_x) \mathbf{B}_z dz \tag{29}$$

and

$$\boldsymbol{\mathcal{R}}^e_z(\widetilde{T}_x, \theta^m) = -\int_{Lz_e} \mathbf{B}_z^T \mathbf{Q}_x(\widetilde{T}_x, \theta^m) dz \tag{30}$$

3.6. Remarks on the resolution of the thermo-mechanical problem

The mechanical problem has been already solved using the variables separation for composite beam structures in [16] and the accuracy and efficiency of the approach has been shown. Thus, the same way is used in the present work with a fourth-order expansion for the z-functions. The resolution of the thermo-mechanical coupling is limited to the computation of the second term of the right hand side of Eq. (5). As the temperature is expressed under a separated form, the computation of this integral can be also divided into 2 parts, one over $\mathcal{B}_x$ and the other one over $\mathcal{B}_z$. Thus, the key point of the method remains available. This computation is given in Section A.

4. Numerical results

In this section, several static tests are presented validating our approach, evaluating its efficiency and showing the properties of the algorithm for the thermal and the thermo-mechanical problems. A classical 8-node quadratic finite element is used for the thermal and mechanical unknowns depending on the x-axis coordinate. For the transverse direction, a fourth-order layer-wise description is chosen.

First, the heat conduction problem is solved. The approach is assessed by comparing with exact solution and LayerWise models including or not the continuity of the transverse heat flux. Then, the thermo-mechanical coupling is considered for different laminated and sandwich beams. Different thermal boundary conditions are also addressed. Their influence on the behavior of the structure is rather important and can make the modeling of such structures difficult. For these tests, the number of dofs is also precised for the two problems associated with the x-function and z-function. They are denoted $Ndof_{\theta x}, Ndof_{\theta z}$ for the thermal unknowns and $Ndof_x, Ndof_z$ for the mechanical unknowns.

Note that the convergence rate of the fixed point process is high. Usually, only less than four iterations are required. This subject is not discussed here.

4.1. Problem of heat conduction in a sandwich media

In this section, several cases are presented to evaluate the efficiency of our approach to solve the thermal problem. The obtained results are assessed by comparing with exact solution from [23], and also LayerWise model with a 2^{nd} order expansion in each layer (See [5]). In this latter, the continuity of the transverse heat flux q_3 at the interface between the layers can be enforced (denoted "LW2-c") or not (denoted "LW2").

4.1.1. Problem 1

A rectangular symmetric sandwich media is considered (see [23]):

geometry: The sandwich is composed by an isotropic core of thickness $h - 2e_f$, and isotropic skins of equal thickness $e_f = 0.2h$. We have $S = \frac{L}{h} = 2$ (very thick beam). It is represented in Fig. 2.

boundary conditions: The structure is submitted to a sinusoidal temperature loading given by $\bar{\theta}_t(x) = \theta_c \sin(\pi x/L)$ at its top edge, with $\theta_c = 1$, while zero temperature is prescribed on the three other edges.

material properties: The conductivity coefficients are $k_{skin} = 0.5$ W/(Km) and $k_{core} = 50.5$ W/(Km).

mesh: N_x is the number of elements over $\mathcal{B}_x$. One numerical layer per physical layer is used. For the separated variable

approach, it corresponds to the number of elements per layer over $\mathcal{B}_z$.

number of dofs: $Ndof_{\theta x} = 2N_x + 1 (= 33 \text{ for } N_x = 16)$ and $Ndof_{\theta z} = 4 * NC + 1 = 13$

results: The temperature is made non-dimensional as $\bar{\theta} = \frac{\theta}{\theta_c}$.

The results are compared with exact solution [23] and LayerWise model with a 2^{nd} order expansion in each layer with and without continuity conditions [5].

First, a convergence study is performed, see Table 1. Two couples are built to obtain the solution. It can be seen that the convergence rate is very high for both temperature and transverse heat flux. Only a $N_x = 4$ mesh for the whole beam is sufficient to obtain the converged value. The heat flux q_1 is more sensitive to the refinement, and a $N_x = 16$ mesh is needed. It will be used hereafter.

Temperature and heat flux distributions along the thickness at $x = L/2$ and $x = L$ are shown in Figs. 3 and 4. The temperature variation is rather important in the top skin of the sandwich. The results of the present approach are in excellent agreement with the reference (exact) solution and are more accurate than the LayerWise models for the transverse heat flux q_3. Numerical results for the heat flux q_1 and q_3 given in Table 2 and Table 3 prove it. In theses tables, -/-/- indicates the number of numerical subdivisions in each layer. The maximum error rate of the present approach is less than 1%. We also notice that these results (with only one numerical layer per physical layer) are similar to the LW2 approach with 4/6/4 numerical layers. The continuity of the transverse heat flux is also fulfilled without any constraints. Thus, the introduction of the variables separation does not decrease the accuracy of the results and the choice of the 4th order expansion in the thickness direction is a key issue. Moreover, the comparison of the number of dofs given in Table 2 and Table 3 shows the very interesting ratio between cost and accuracy of the present approach.

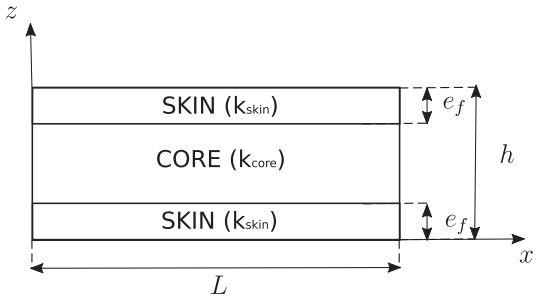

Fig. 2. Rectangular sandwich media.

Table 1
Convergence study – Problem 1.

N_x	$\bar{\theta}(L/2, 0.8h)$	$q_1(L/2, h/2)$	$q_3(L, h)$
2	3.936E−02	2.705	−2.486
4	3.956E−02	2.454	−2.484
8	3.957E−02	2.371	−2.484
16	3.957E−02	2.349	−2.484
32	3.957E−02	2.344	−2.484

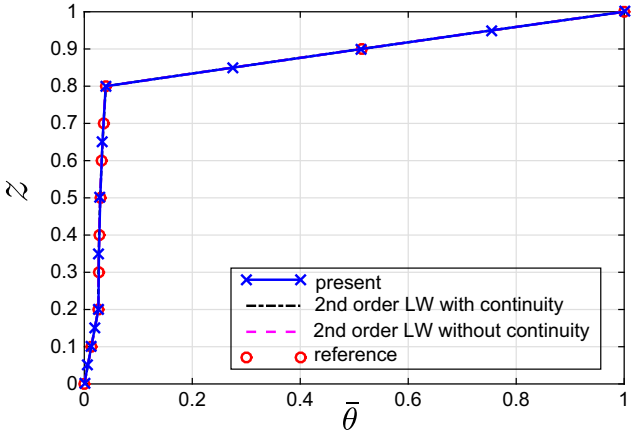

Fig. 3. Distribution of temperature across the thickness at $x = L/2$ – Problem 1.

4.1.2. Problem 2

The second thermal problem is described as follows:

geometry: A three-layer sandwich beam with graphite-epoxy faces and a soft core with thickness $e = 0.1h$ is considered (Cf. [10]). $S = \frac{L}{h} = 10$.

boundary conditions:constrained opposite temperature on the top and the bottom surfaces of the beam such as: $\theta(x, h/2) = -\theta(x, -h/2) = \theta_{max} \sin(\pi x/L)$

material properties: The orientation of all the plies is $\gamma_k = 0, k = 1, 2, 3$. for the face: $\lambda_L = 1.5\ \mathrm{Wm^{-1}K^{-1}}$, $\lambda_T = 0.5\ \mathrm{Wm^{-1}\ K^{-1}}$ where L refers to the fiber direction, T refers to the transverse direction.

for the core: $\lambda_1 = \lambda_3 = 3.0\ \mathrm{Wm^{-1}\ K^{-1}}$

mesh: $N_x = 16$, one numerical layer per physical layer is used.

results: The results are compared with exact solution [23] and LayerWise model with a 2^{nd} order expansion in each layer with and without continuity conditions [5].

The solution is obtained with four couples. The couples (T_x^i, T_z^i) are represented in Fig. 5. The first couple allows to ensure the prescribed temperature on the structure and T_x is parabolic along x while T_z is equal to -1 at the bottom and $+1$ at the top. It must be denoted that the variation across the thickness is linear per layer. The second one is a global correction. Then, the third and fourth ones bring a local correction near the edge of the beam. The distribution of the associated z-functions through the thickness becomes more complex. The resulting distribution of the temperature across the thickness are the same as the reference solution (see Fig. 6). Again, it should be noticed that the distribution of the transverse heat flux is very accurate with only one numerical layer per physical layer for the present model with a fourth-order z-expansion. The continuity of the transverse heat flux is satisfied whereas it must be constrained for the LW2 model (Fig. 7 right). Moreover, in this later, 2/6/2 numerical layers (620 dofs) are needed to be close to the reference solution. Thus, the importance of the z-expansion order is highlighted.

4.2. Thermo-mechanical analysis

4.2.1. Sandwich beam

The thermo-mechanical analysis of the sandwich beam described in Section 4.1.2 is performed. It is detailed below:

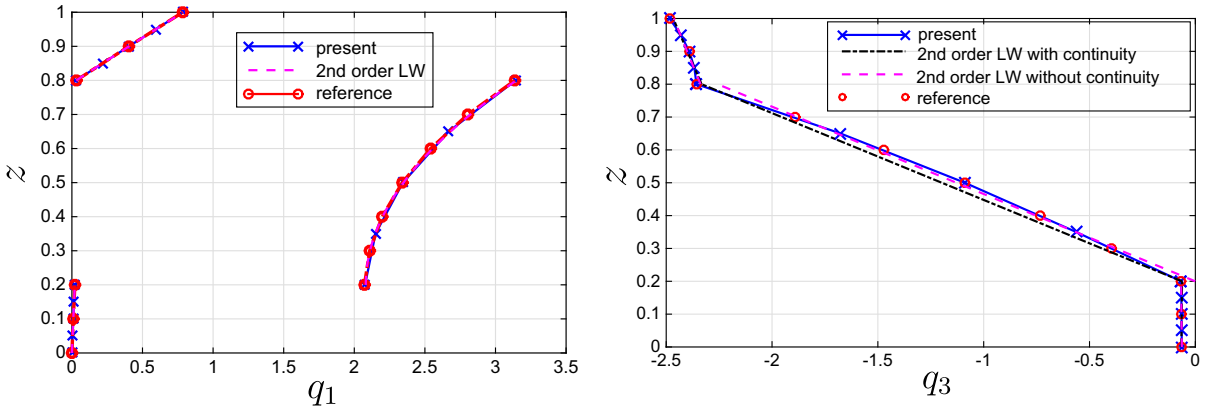

Fig. 4. Distribution of heat flux q_1 and q_3 across the thickness at $x = L$ (left) and $x = L/2$ (right) – Problem 1.

Table 2
heat flux q_1 across the thickness – $N_x = 16$ – Problem 1.

	z	Present 1/1/1	LW2-c 1/1/1	LW2 4/6/4	Exact
1st layer	0	0.00	0.000	0.000	0
	0.1	0.010	0.010	0.010	0.010
	0.2^-	0.021	0.020	0.021	0.021
2nd layer	0.2^+	2.081	2.050	2.081	2.072
	0.5	2.349	2.348	2.349	2.340
	0.8^-	3.149	3.182	3.149	3.137
3rd layer	0.8^+	0.031	0.032	0.031	0.031
	0.9	0.405	0.404	0.405	0.403
	1	0.788	0.788	0.788	0.785
d.o.f.		33 + 13	62	868	–

Table 3
heat flux q_3 across the thickness – $N_x = 16$ – Problem 1.

	z	Present	LW2-c	LW2		Exact
		1/1/1	1/1/1	2/3/2	4/6/4	
1st layer	0	−0.064	−0.066	−0.064	−0.064	−0.065
	0.1	−0.065	−0.064	−0.065	−0.065	−0.066
	0.2^-	−0.067	−0.063	−0.067	−0.067	−0.068
2nd layer	0.2^+	−0.067	−0.063	−0.064	−0.066	−0.068
	0.5	−1.089	−1.198	−1.094	−1.087	−1.089
	0.8^-	−2.357	−2.333	−2.340	−2.354	−2.356
3rd layer	0.8^+	−2.357	−2.333	−2.352	−2.356	−2.356
	0.9	−2.391	−2.400	−2.386	−2.390	−2.390
	1	−2.484	−2.467	−2.479	−2.483	−2.483
d.o.f.		33 + 13	62	434	868	–

geometry: thick sandwich beam with $S = 5$
boundary conditions: simply-supported beam
material properties: for the face
$Y_L = 131.1$ GPa, $Y_T = 6.9$ GPa, $G_{LT} = 3.588$ GPa, $G_{TT} = 2.3322$ GPa, $\nu_{LT} = 0.32$, $\nu_{TT} = 0.49$, $\alpha_L = 0.0225\ 10^{-6}\ \mathrm{K}^{-1}$, $\alpha_T = 22.5\ 10^{-6}\ \mathrm{K}^{-1}$,
for the core
$E_1 = 0.2208$ MPa, $E_2 = 0.2001$ MPa, $E_3 = 2760$ MPa, $G_{12} = 16.56$ MPa, $G_{23} = 455.4$ MPa, $G_{13} = 545.1$ MPa, $\nu_{12} = 0.99$, $\nu_{13} = 3\ 10^{-5}$, $\nu_{23} = 3\ 10^{-5}$, $\alpha_1 = \alpha_3 = 30.6\ 10^{-6}\ \mathrm{K}^{-1}$
mesh: half of the beam is meshed using N_x FE along x-direction. N_f, N_c are the number of elements in the face and in the core, respectively. For the present method, they are related to the 1D mesh over $\mathcal{B}_z$, while it is associated to the number of 2D elements along z-direction for the 2D FEM analysis from ANSYS.
results: The results $(\bar{u}, \bar{w}, \bar{\sigma}_{11}, \bar{\sigma}_{13})$ are nondimensionalised using: $\bar{u} = \frac{100u_1}{\alpha_T S h \theta_{max}}$, $\bar{w} = \frac{100u_3}{\alpha_T S^2 h \theta_{max}}$, $\bar{\sigma}_{11} = \frac{\sigma_{11}}{\alpha_T E_T \theta_{max}}$, $\bar{\sigma}_{13} = \frac{S\sigma_{13}}{\alpha_T E_T \theta_{max}}$. The results are compared with 2D FEM analysis using ANSYS with plane stress assumptions. The eight-node element PLANE77 is used for the thermal part and PLANE183 for the mechanical analysis.

First, a convergence study is carried out for both ANSYS modeling and the present approach. For the 2D FEM analysis, the results are summarized in Table 4 varying N_x with a fixed value of N_f and N_c, and varying N_f and N_c for a fixed value of N_x. A very refined mesh is needed to obtain satisfactory results. The convergence of the transverse displacement and the in-plane stress wrt N_x is greater than those of the in-plane displacement at the end of the beam. A $N_x = 512$ mesh can be retained. The transverse shear stress is more sensitive to the thickness refinement. $N_f = N_c = 32$ drives to a converged value. Moreover, the location of the maximum of $\bar{\sigma}_{13}$ is close to the top or bottom surface, which implies to have a refined description through the thickness with a suitable mesh.

The same study is performed for the variables separation approach. It is shown in Table 5. The same comments can be made. From this table, it can be inferred that a $N_x = 128$ mesh with $N_f = 4, N_c = 4$ can be used. So, the convergence rate is higher for the present approach.

As already proposed in [24], an alternative thickness refinement consists in discretizing the z-functions using 4 elements in the face with smaller size near the top surface and the layer interface, namely $\frac{h}{100}$ / $\frac{h}{25}$ /$\frac{h}{25}$/$\frac{h}{100}$. The associated numerical results are denoted $N_f = 4$ (sr) in Table 5. 14 couples are built to obtain the mechanical response. The maximum error rate is less than 2% when compared to 2D FEM results from ANSYS. For further comparison, the distribution of the displacements and the stresses through the thickness are also shown in Figs. 8 and 9. The results are in very good agreement with the reference solution. A zig-zag effect occurs for the axial displacement and the transverse displacement is non-linear. The distribution of the transverse shear stress in the face is rather complex. The maximum value is located near the free top/bottom surface, which makes difficult to recover the free boundary conditions. Nevertheless, it is nearly satisfied with the present model by using suitable numerical layers. It should be noted that the 2D FE results need also a high refinement.

From a computational point of view, the 2D ANSYS model implies about 300.000 dofs with a bandwidth of the linear system equal to 586, whereas only $Ndof_x = 514/Ndof_z = 98$ dofs are involved in the

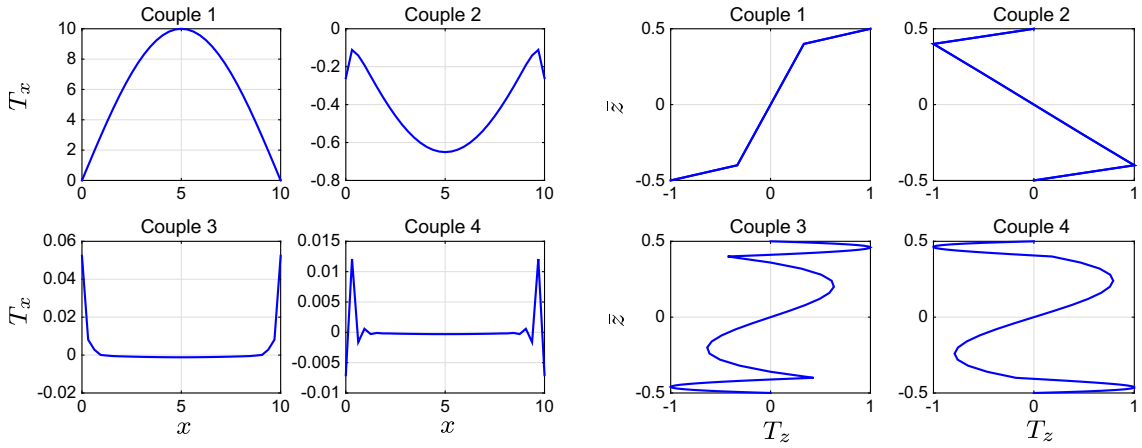

Fig. 5. Distribution of the x-functions T_x^i and z-functions T_z^i – Problem 2.

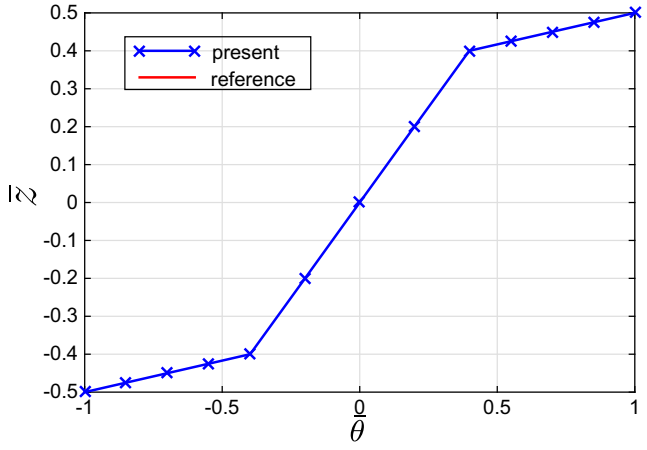

Fig. 6. Distribution of temperature across the thickness at $x = L/2$ – Problem 2.

Table 4
Convergence study (2D FEM ANSYS).

	$\bar{u}_{max}$	$\bar{w}_{max}$	$\bar{\sigma}_{11max}$	$\bar{\sigma}_{13max}(\bar{z})$
Convergence wrt N_x with $N_f = N_c = 4$				
$N_x = 32$	0.196	0.5331	0.0319	0.159 (-0.475)
$N_x = 64$	0.202	0.5331	0.0318	0.176 (-0.475)
$N_x = 128$	0.223	0.5331	0.0318	0.181 (-0.475)
$N_x = 256$	0.237	0.5331	0.0318	0.181 (-0.475)
$N_x = 512$	0.245	0.5331	0.0318	0.180 (-0.475)
$N_x = 1024$	0.249	0.5331	0.0318	0.180 (-0.475)
Convergence wrt N_f, N_c with $N_x = 512$				
$N_f = N_c = 4$	0.245	0.5331	0.0318	0.180 (-0.475)
$N_f = N_c = 8$	0.248	0.5331	0.0321	0.189 (-0.487)
$N_f = N_c = 16$	0.246	0.5331	0.0322	0.178 (-0.487)
$N_f = N_c = 32$	0.246	0.5331	0.0322	0.176 (-0.485)
$N_f = N_c = 48$	0.246	0.5331	0.0322	0.176 (-0.485)

x and z problems of the variables separation approach with a bandwidth of 6. Moreover, as shown previously, the refinement of the description of the solution through the thickness is needed. For that, it is also necessary to refine the mesh in the x-direction in the 2D FEM to ensure a correct size ratio of the elements. Thus, the refinement in one direction has an influence on the other direction. That is not the case in the present work where the size of elements of the two problems (x and z functions) is independent. So, all these features make this approach very efficient.

4.2.2. A symmetric four-layer beam

In this section, a symmetric laminated composite beam taken from [10] is considered:

geometry: Composite cross-ply beam $[0°/90°/90°/0°]$ with $S = 5, 10$. Each layer has the same thickness ($h/4$).

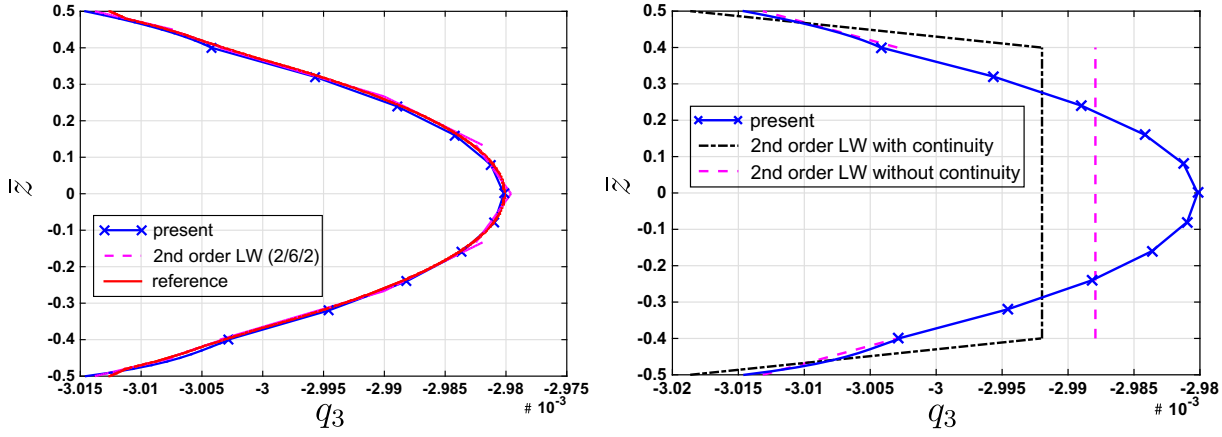

Fig. 7. Distribution of heat flux q_3 along the thickness with and without continuity (right), and with sub-layers (left) – Problem 2.

Table 5
Convergence study – variable separation approach.

	$\bar{u}_{max}$	$\bar{w}_{max}$	$\bar{\sigma}_{11max}$	$\bar{\sigma}_{13max}(\bar{z})$
Convergence wrt N_x *with* $N_f = N_c = 1$				
$N_x = 16$	0.195	0.5334	0.0323	0.102 (-0.465)
$N_x = 32$	0.203	0.5336	0.0323	0.130 (-0.470)
$N_x = 64$	0.197	0.5336	0.0322	0.147 (-0.475)
$N_x = 128$	0.187	0.5335	0.0322	0.154 (-0.475)
$N_x = 256$	0.185	0.5335	0.0322	0.156 (-0.480)
Convergence wrt N_f, N_c *with* $N_x = 128$				
$N_f = 1, N_c = 1$	0.187	0.5335	0.0322	0.154 (-0.475)
$N_f = 2, N_c = 2$	0.251	0.5328	0.0321	0.166 (-0.480)
$N_f = 4, N_c = 4$	0.251	0.5325	0.0319	0.167 (-0.475)
$N_f = 4$ (sr), $N_c = 4$	0.241	0.5332	0.0322	0.171 (-0.484)

boundary conditions: Two thermal loads are prescribed:

TC1: $\theta(x, h/2) = -\theta(x, -h/2) = \theta_{max}\ \sin(\pi x/L)$
TC2: zero temperature $\theta(x, z)$ at $x = 0$ and $x = L$
$\theta(x, h/2) = -\theta(x, -h/2) = \theta_{max}\ \sin(\pi x/L)$
Mechanical BC: simply-supported beam.
material properties: $E_L = 181$ GPa, $E_T = 10.3$ GPa, $G_{LT} = 7.17$ GPa, $G_{TT} = 2.87$ GPa, $\nu_{LT} = 0.28$, $\nu_{TT} = 0.33$, $\alpha_L = 0.02\ 10^{-6}\ \mathrm{K}^{-1}$, $\alpha_T = 22.5\ 10^{-6}\ \mathrm{K}^{-1}$, $\lambda_L = 1.5\ \mathrm{Wm}^{-1}\mathrm{K}^{-1}$, $\lambda_T = 0.5\ \mathrm{Wm}^{-1}\mathrm{K}^{-1}$.

mesh: half of the beam is meshed.
results: The results $(\bar{u}, \bar{w}, \bar{\sigma}_{11}, \bar{\sigma}_{13})$ are made nondimensional as in Section 4.2.1. The results are compared with 2D FEM analysis using ANSYS with plane stress assumptions and converged mesh from the previous section.

For TC1, 4 and 10 couples are built for the thermal and mechanical solution, respectively. The distribution of the temperature over the whole beam and at $x = 0, x = L/2$ is shown in Figs. 10(a), (b) and 12. The variation is linear in the middle of the beam, but not linear at the end. For further comparison, a zoom on the temperature distribution is shown in Fig. 11(a) and (b). The distributions are very close to the reference solution. The accuracy of the induced displacements and stresses are assessed in Table 6. The maximum error rate is 1.3%. The distributions of the displacements and stresses are also presented in Figs. 13 and 14. It is seen that the present work performs very well when compared with the reference solution. High variation of the slope occurs for the in-plane displacement. We also observe that the variation of the in-plane stress is non-linear in the 0° layers. For the transverse shear stress, steep gradient occurs near the two free surfaces and the 0°/90° interface. It seems that a singularity exists at the interface. This is well-captured by using numerical layers as in the previous section. The accuracy of the results can be improved by using 6/4/4/6 numerical layers per physical layer instead of 1/1/1/1 discretiza-

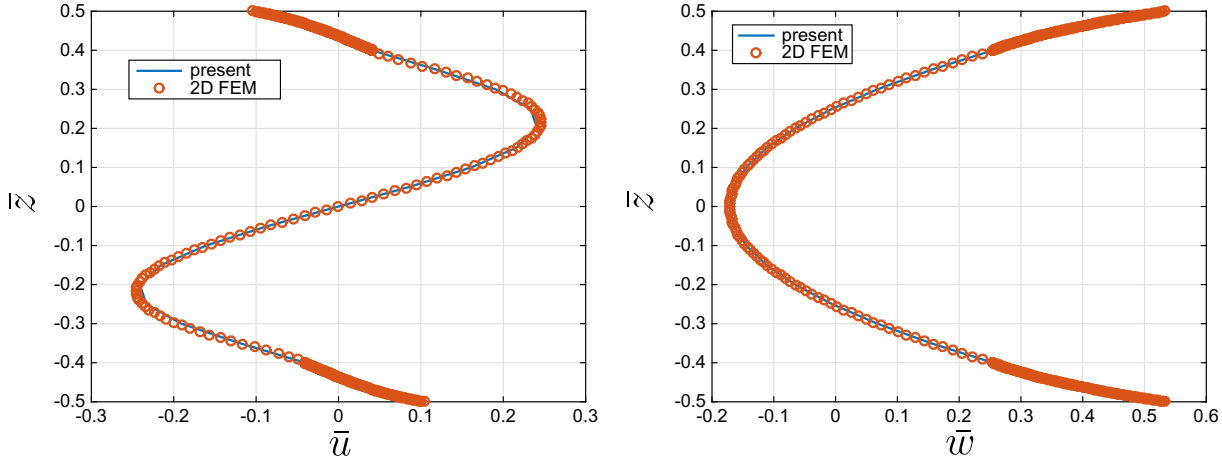

Fig. 8. Distribution of $\bar{u}$ (left) and $\bar{w}$ (right) along the thickness – $S = 5$ – sandwich beam – $N_f = 4$ (sr), $N_c = 4$.

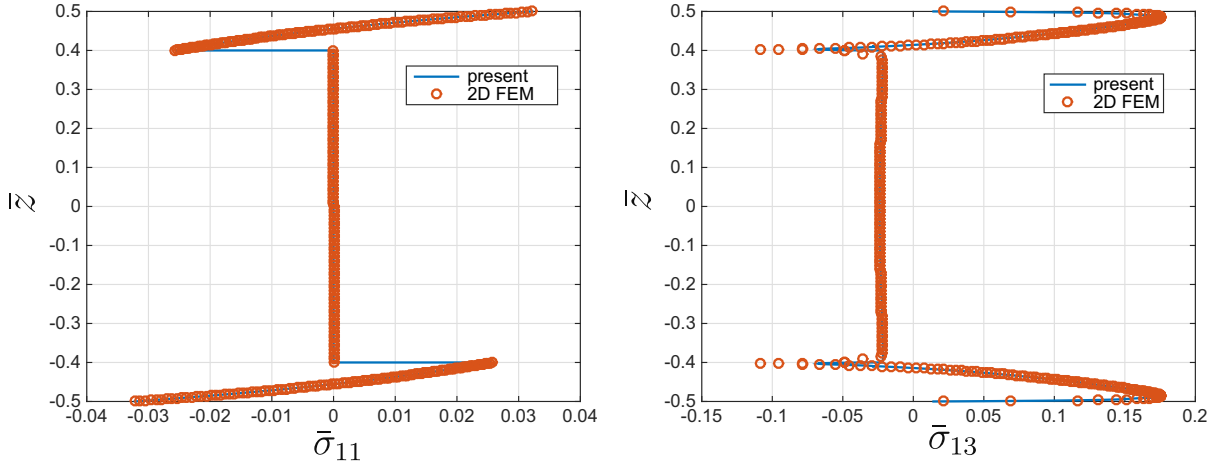

Fig. 9. Distribution of $\bar{\sigma}_{11}$ (left) and $\bar{\sigma}_{13}$ (right) along the thickness – $S = 5$ – sandwich beam – $N_f = 4$ (sr), $N_c = 4$.

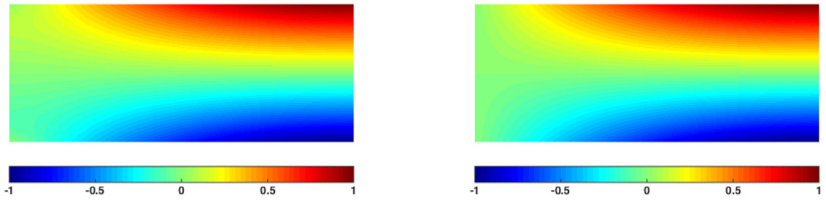

(a) present - TC1 (b) 2D FEM Ansys - TC1

(c) present - TC2 (d) 2D FEM Ansys - TC2

Fig. 10. Distribution of temperature – $S = 5$–4 layers $[0^\circ/90^\circ/90^\circ/0^\circ]$.

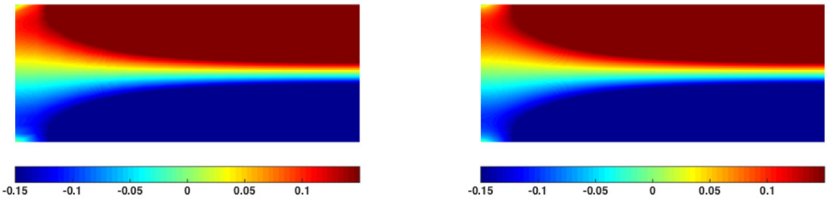

(a) present - TC1 (b) 2D FEM Ansys - TC1

(c) present - TC2 (d) 2D FEM Ansys - TC2

Fig. 11. Distribution of temperature with a scale over $[-0.15, 0.15]$ – $S = 5$–4 layers $[0^\circ/90^\circ/90^\circ/0^\circ]$.

tion, as shown in Fig. 15. The free boundary conditions on the top and bottom surfaces are also nearly recovered despite the challenging test case.

As far as the TC2 is concerned, only two couples are sufficient for the temperature and one couple for the mechanical solution. The temperature distribution over the structure is compared with

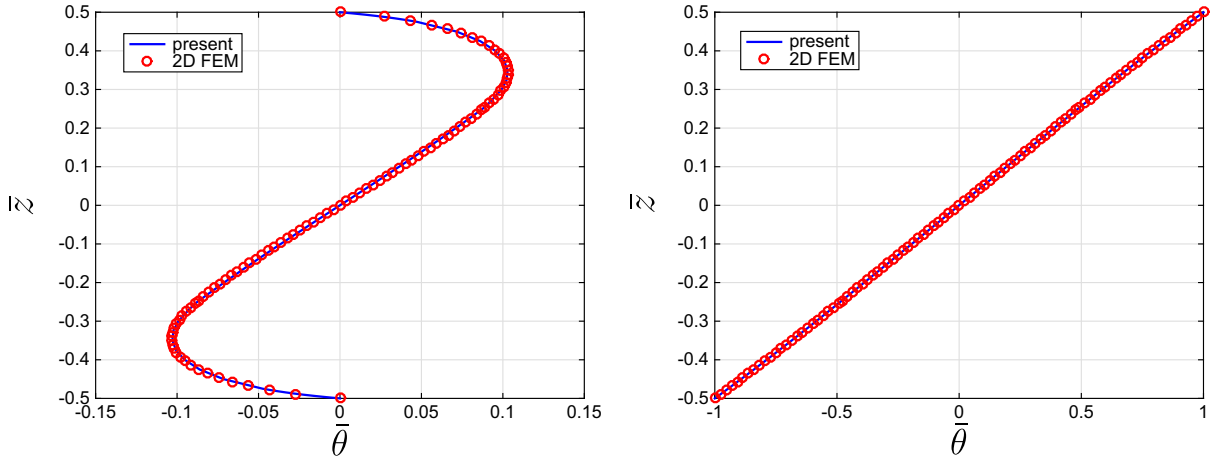

Fig. 12. Distribution of temperature along the thickness at $x = 0$ (left) and $x = L/2$ (right) – $S = 5$–4 layers $[0^\circ/90^\circ/90^\circ/0^\circ]$ – TC1.

Table 6
4 layers $[0^\circ/90^\circ/90^\circ/0^\circ]$ – TC1.

	Present	Error	2D FEM
$\bar{u}(0,-h/2)$	0.4386	0.9%	0.4426
$\bar{w}(L/2,-h/2)$	0.8663	0.0%	0.8860
$\bar{\sigma}_{11}(L/2,-h/4)$	0.7112	1.3%	0.7207
$\bar{\sigma}_{13}(0,0)$	−0.4791	1.2%	−0.4731

a reference solution in Figs. 10(c), (d) and 11(c), (d). It can be inferred from these figures that the agreement with the reference solution is very good. Table 7 shows that the present model is very efficient and accurate for very thick and moderately thick beam. The maximum error rate is less than 0.3%. It is confirmed by showing the distribution of the displacements, the axial, transverse

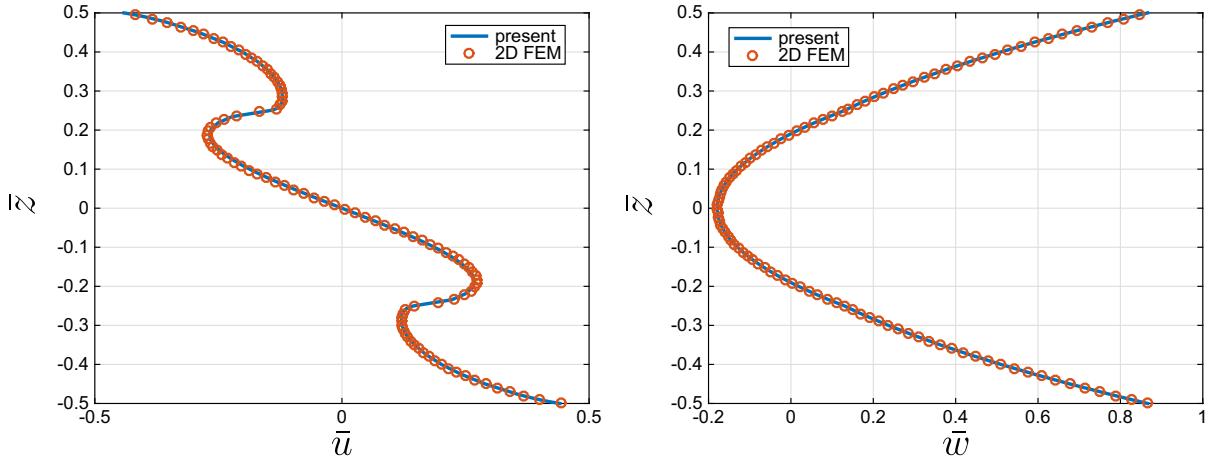

Fig. 13. Distribution of $\bar{u}$ (left) and $\bar{w}$ (right) along the thickness – $S = 5$–4 layers $[0^\circ/90^\circ/90^\circ/0^\circ]$ – TC1.

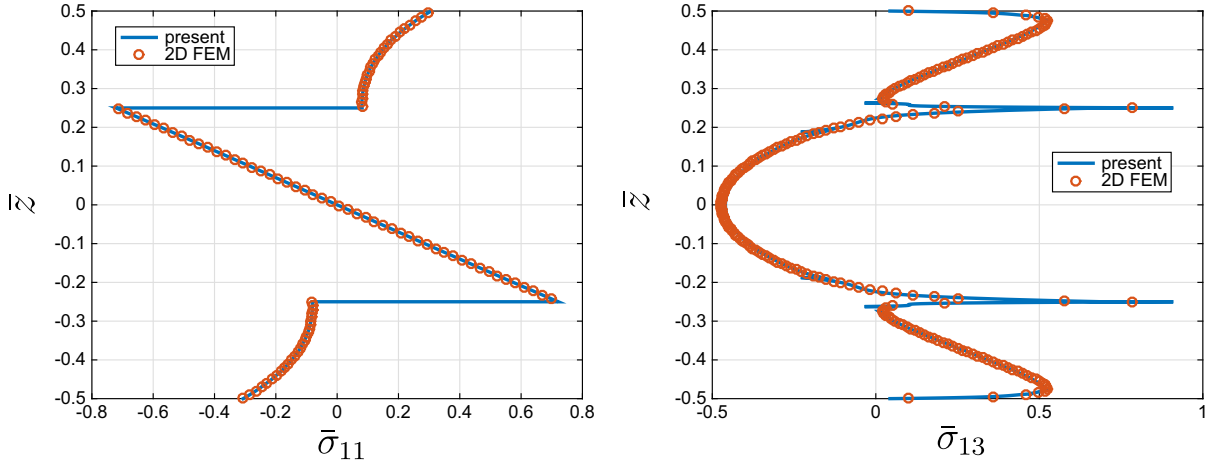

Fig. 14. Distribution of $\bar{\sigma}_{11}$ (left) and $\bar{\sigma}_{13}$ (right) along the thickness – $S = 5$–4 layers $[0^\circ/90^\circ/90^\circ/0^\circ]$ – TC1.

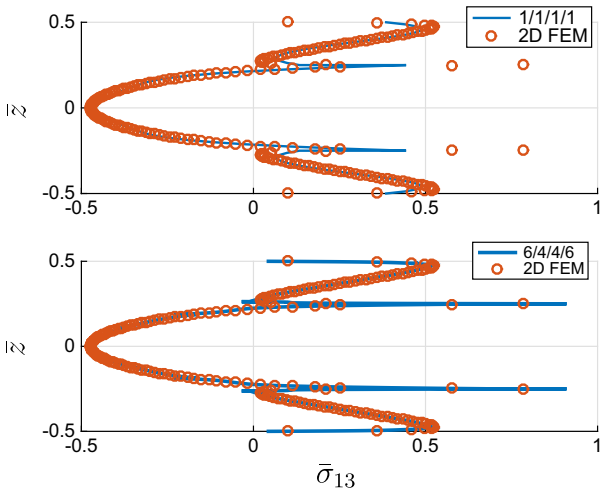

Fig. 15. Distribution of $\bar{\sigma}_{13}$ (right) along the thickness – $S = 5$–4 layers – 1/1/1/1 and 6/4/4/6 Numerical layers – TC1.

shear and normal stresses in Figs. 16 and 17. It can be seen that the physical requirements are fulfilled.

This test case illustrates also the influence of the thermal boundary conditions on the mechanical response. Even though the temperature distribution seems to be similar (Fig. 10(a) and (c)) for the two test cases, rather small discrepancies can be observed (Fig. 11(a) and (c)). These ones make the transverse shear stress distribution through the thickness very different (see Figs. 14 (right) and 17(middle)). It appears that TC2 is less challenging than TC1.

5. Conclusion

In this article, a beam finite element based on the variables separation has been presented and evaluated through different benchmarks for thermo-mechanical problems. This method has been applied to the modeling of both laminated and sandwich composite. The temperature and displacement are expressed as a separated representation of two 1D functions. The axial functions have a quadratic interpolation. For the transverse functions, a

Table 7
4 layers $[0^\circ/90^\circ/90^\circ/0^\circ]$ - TC2.

		$\bar{u}(0, h/2)$	$\bar{w}(L/2, 0)$	$\bar{w}(L/2, h/2)$	$\bar{\sigma}_{11}(L/2, -h/4^+)$	$\bar{\sigma}_{13}(0, 0)$	$\bar{\sigma}_{33}$max
5	Present	−0.4003 (0.0 %)	−0.1795 (0.1 %)	0.8651 (0.0 %)	0.7207 (0.0 %)	−0.1657 (0.0 %)	1.3316 (0.2 %)
	2D FEM	−0.4004	−0.1794	0.8652	0.7207	−0.1657	1.3337
10	Present	−0.3151 (0.0 %)	0.0904 (0.1 %)	0.3559 (0.0 %)	0.7349 (0.0 %)	−0.1659 (0.1 %)	0.6585 (0.3 %)
	2D FEM	−0.3152	0.0905	0.3560	0.7349	−0.1661	0.6605

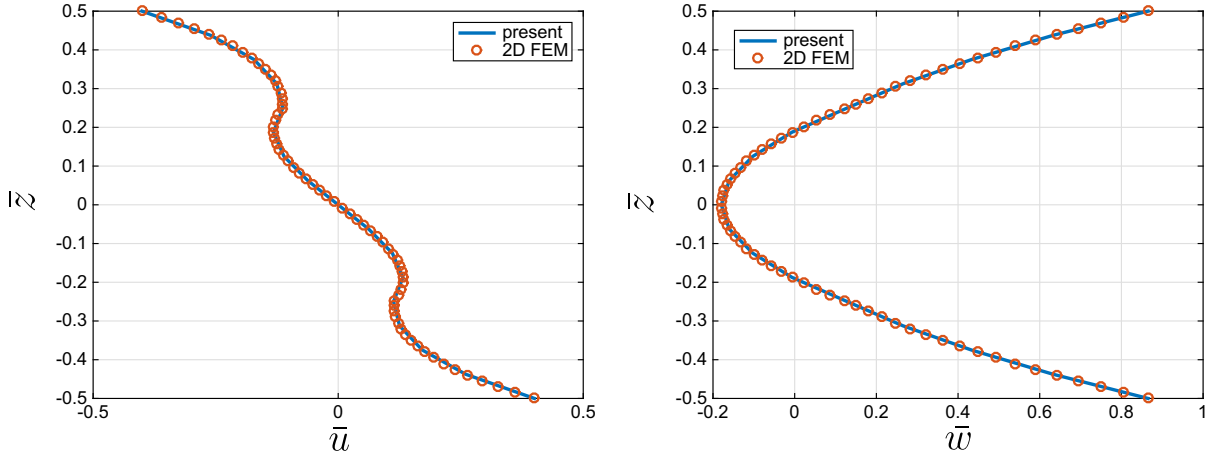

Fig. 16. Distribution of $\bar{u}$ (left) and $\bar{w}$ (right) along the thickness – $S = 5$–4 layers $[0^\circ/90^\circ/90^\circ/0^\circ]$ – TC2.

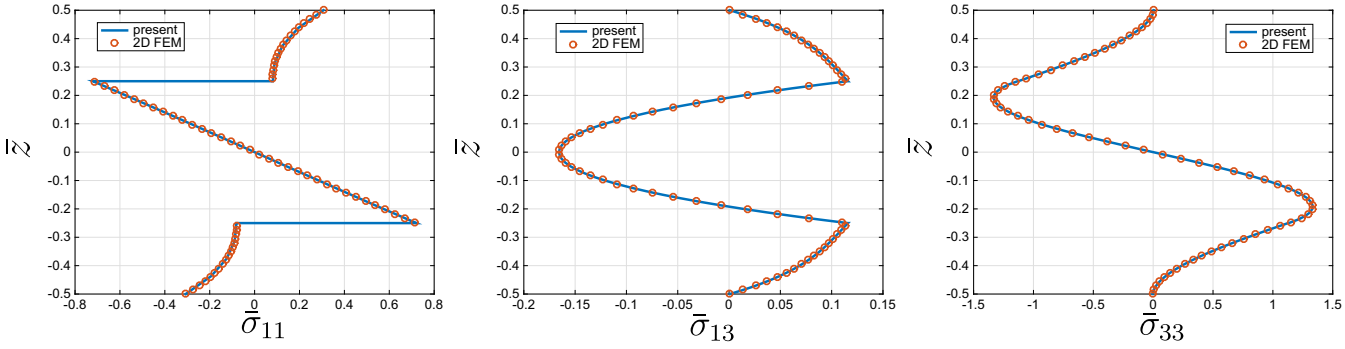

Fig. 17. Distribution of $\bar{\sigma}_{11}$ (left) and $\bar{\sigma}_{13}$ (right) along the thickness – $S = 5$–4 layers $[0^\circ/90^\circ/90^\circ/0^\circ]$ – TC2.

fourth-order expansion are considered. The derived iterative process implies the resolution of 1D problems and each of them has a low computational cost. The total cost depends on the number of couples used to represent the solution.

This study has showed the interesting capability of the method to solve the coupling problem. As in the mechanical analysis, it has been emphasized the importance of the choice of the z-expansion order for such structures. The thermal effect can cause complex behavior on the mechanical response which is needed to modelise with accuracy. It has been shown that complex shape functions in the transverse direction can be built for the temperature. Then, the excellent accuracy on the thermal response allows us to obtain accurate mechanical results. Moreover, this approach is very interesting from a computational point of view, especially in the framework of LW approach. Indeed, only 1D problems with few dofs are involved in this analysis. Finally, we have proved that it is particularly suitable to model laminated and sandwich composite beam.

Based on these promising results, the use of the method for plate and shell structures will be carried out in the framework of multi-fields analysis.

Appendix A. Thermo-mechanical load

The computation of the second term of the right hand side of Eq. (5) is detailed here. It is denoted $I_{thme} = \int \int_{\mathcal{B}} \delta\boldsymbol{\varepsilon}^T \overline{\mathbf{C}}^{(k)} \bar{\boldsymbol{\alpha}}^{(k)} \Delta\theta \; dV$. In the following, the notations defined in [16] are used. As in the thermal part, two problems have to be solved. We recall that

$$\varepsilon(\bar{\mathbf{f}} \circ \mathbf{v}) = \mathbf{B}_z(\bar{f})\mathcal{E}_v \text{ with } \mathcal{E}_v^e = \mathbf{B}_x^{mech}\mathbf{q}_e^v \tag{A.1}$$

and

$$\varepsilon(\bar{\mathbf{v}} \circ \mathbf{f}) = \mathbf{B}_x(\bar{v})\mathcal{E}_f \text{ with } \mathcal{E}_f^e = \mathbf{B}_z^{mech}\mathbf{q}_e^f \tag{A.2}$$

The matrices $\mathbf{B}_x$ and $\mathbf{B}_z$ contain the interpolation functions, their derivatives and the jacobian components dependent on the chosen discrete representation. The elementary vector of degree of freedom (dof) associated with the finite element mesh in $\mathcal{B}_x$ and $\mathcal{B}_z$ is denoted $\mathbf{q}_e^v$ and $\mathbf{q}_e^f$, respectively.

A.1. Finite element problem to be solved on $\mathcal{B}_x$

Using Eq. (A.1) and the expression of the temperature under the separated form given in Eq. (6), I_{thme} can be written as

$$I_{thme} = \int_{\mathcal{B}_x} \delta\mathcal{E}_v^T \underbrace{\int_{\mathcal{B}_z} \mathbf{B}_z^T(\bar{f})\overline{\mathbf{C}}^{(k)}\bar{\boldsymbol{\alpha}}^{(k)} T_z^i(z)\, dz}_{\mathbf{f}_{thme_z}^i} T_x^i(x)\, dx \tag{A.3}$$

Thus, the elements' thermo-mechanical load is deduced:

$$\mathbf{F}_{thme_z}^e(\bar{f}) = \sum_{i=1}^{N} \int_{L_e} \mathbf{B}_x^{mech^T} \mathbf{f}_{thme_z}^i T_x^i(x)\, dx \tag{A.4}$$

A.2. Finite element problem to be solved on $\mathcal{B}_z$

Using Eqs. (A.2) and (6), we have

$$I_{thme} = \int_{\mathcal{B}_z} \delta\mathcal{E}_f^T \underbrace{\int_{\mathcal{B}_x} \mathbf{B}_x^T(\bar{v})\overline{\mathbf{C}}^{(k)}\bar{\boldsymbol{\alpha}}^{(k)} T_x^i(x)\, dx}_{\mathbf{f}_{thme_x}^{(k)^i}} T_z^i(z)\, dz \tag{A.5}$$

Thus, the elements' thermo-mechanical load is deduced:

$$\mathbf{F}_{thme_x}^e(\bar{v}) = \sum_{i=1}^{N} \int_{z_e} \mathbf{B}_z^{mech^T} \mathbf{f}_{thme_x}^{(k)^i} T_z^i(z)\, dz \tag{A.6}$$

References

[1] Robaldo A. Finite element analysis of the influence of temperature profile on thermoelasticity of multilayered plates. Comput Struct 2006;84:1236–46.
[2] Tanigawa Y, Murakami H, Ootao Y. Transient thermal stress analysis of a laminated composite beam. J Therm Stresses 1989;12:25–39.
[3] Blandford G, Tauchert T, Du Y. Self-strained piezothermoelastic composite beam analysis using first-order shear deformation theory. Compos Part B: Eng J 1999;30(1):51–63.
[4] Reddy J. Mechanics of laminated composite plates – theory and analysis. Boca Raton, FL: CRC Press; 1997.
[5] Vidal P, Polit O. A thermomechanical finite element for the analysis of rectangular laminated beams. Finite Elem Anal Des 2006;42(10):868–83. http://dx.doi.org/10.3166/reef.11.379-392.
[6] Lee H-J, Saravanos D. Coupled layerwise analysis of thermopiezoelectric composite beams. AIAA J 1996;34(6):1231–7.
[7] Carrera E. An assessment of mixed and classical theories for the thermal stress analysis of orthotropic multilayered plates. J Therm Stresses 2000;23:797–831.
[8] Carrera E, Ciuffreda A. Closed-form solutions to assess multilayered-plate theories for various thermal stress problems. J Therm Stresses 2004;27:1001–31.
[9] Giunta G, Metla N, Belouettar S, Ferreira A, Carrera E. A thermo-mechanical analysis of isotropic and composite beams via collocation with radial basis functions. J Therm Stresses 2013;36(11):1169–99.
[10] Kapuria S, Dumir P, Ahmed A. An efficient higher order zigzag theory for composite and sandwich beams subjected to thermal loading. Int J Solids Struct 2003;40:6613–31.
[11] Lezgy-Nazargah M. Fully coupled thermo-mechanical analysis of bi-directional FGM beams using NURBS isogeometric finite element approach. Aerosp Sci Tech 2015;45:154–64.
[12] Hetnarski R, Eslami M. Thermal stresses – advanced theory and applications. Springer; 2009.
[13] Tauchert T. Thermally induced flexure, buckling and vibration of plates. Appl Mech Rev 1991;44(8):347–60.
[14] Noor A, Burton W. Computational models for high-temperature multilayered composite plates and shells. Appl Mech Rev 1992;45(10):419–46.
[15] Ammar A, Mokdada B, Chinesta F, Keunings R. A new family of solvers for some classes of multidimensional partial differential equations encountered in kinetic theory modeling of complex fluids. J Non-Newtonian Fluid Mech 2006;139:153–76.
[16] Vidal P, Gallimard L, Polit O. Assessment of a composite beam finite element based on the proper generalized decomposition. Compos Struct 2012;94 (5):1900–10. http://dx.doi.org/10.1016/j.compstruct.2011.12.016.
[17] Savoia M, Reddy J. A variational approach to three-dimensional elasticity solutions of laminated composite plates. J Appl Mech ASME 1992;59:166–75.
[18] Bognet B, Bordeu F, Chinesta F, Leygue A, Poitou A. Advanced simulation of models defined in plate geometries: 3D solutions with 2D computational complexity. Comput Methods Appl Mech Eng 2012;201–204:1–12. http://dx.doi.org/10.1016/j.cma.2011.08.025.
[19] Vidal P, Gallimard L, Polit O. Proper generalized decomposition and layer-wise approach for the modeling of composite plate structures. Int J Solids Struct 2013;50(14-15):2239–50. http://dx.doi.org/10.1016/j.ijsolstr.2013.03.034.
[20] Pruliere E, Chinesta F, Ammar A, Leygue A, Poitou A. On the solution of the heat equation in very thin tapes. Int J Therm Sci 2013;65:148–57.
[21] Nouy A. A priori model reduction through proper generalized decomposition for solving time-dependent partial differential equations. Comput Methods Appl Mech Eng 2010;199(23–24):1603–26.
[22] Chinesta F, Ammar A, Leygue A, Keunings R. An overview of the proper generalized decomposition with applications in computational rheology. J Non-Newtonian Fluid Mech 2011;166(11):578–92.
[23] Blanc M, Touratier M. A constrained discrete layer model for heat conduction in laminated composites. Comput Struct 2005;83(21–22):1705–18.
[24] Saeedi N, Sab K, Caron J-F. Delaminated multilayered plates under uniaxial extension. part ii: efficient layerwise mesh strategy for the prediction of delamination onset. Int J Solids Struct 2012;49:3727–40.